

Advances in Space Radiation Transport Codes

J. W. Wilson^{1*}, J. Tweed², J. H. Heinbockel², R.K. Tripathi¹, F. A. Cucinotta³, W. Schimmerling⁴

¹NASA Langley Research Center, Hampton, VA 23681 USA,

²Old Dominion University, Norfolk, VA 23529 USA

³NASA Johnson Space Center, Houston, TX 77058 USA,

⁴NASA Headquarters, Washington, DC 20546 USA

*Corresponding author: Phone, +757-864-1414, Fax; +757-864-8094, E-mail;

john.w.wilson@larc.nasa.gov

Early space radiation shield code development relied on Monte Carlo methods and made important contributions to past space activity. The disadvantage was that slow computational procedures relegated shield evaluation near the end of the design process followed by off-optimum solutions to shielding issues. We have been investigating high-speed computational procedures to allow shield analysis from the preliminary engineering concept to the final design. For the last few decades, we have pursued deterministic solutions of the Boltzmann equation using marching procedures allowing field mapping within the International Space Station (ISS) in tens of minutes using standard Finite Element Method (FEM) geometry common to engineering design methods. Current interest is in developing Green's function methods allowing laboratory validation of computational procedures and database, as well as, the direct laboratory validation of engineering material radiation transmission properties for evaluation of new engineering concepts.

The relevant transport equations are the linear Boltzmann equations for the flux density $\phi_j(\mathbf{x}, \boldsymbol{\Omega}, E)$ for particle type j and are written as

$$\boldsymbol{\Omega} \cdot \nabla \phi_j(\mathbf{x}, \boldsymbol{\Omega}, E) = \sum_k \sigma_{jk}(\boldsymbol{\Omega}, \boldsymbol{\Omega}', E, E') \phi_k(\mathbf{x}, \boldsymbol{\Omega}', E') d\boldsymbol{\Omega}' dE' - \sigma_j(E) \phi_j(\mathbf{x}, \boldsymbol{\Omega}, E) \quad (1)$$

where $\sigma_j(E)$ and $\sigma_{jk}(\boldsymbol{\Omega}, \boldsymbol{\Omega}', E, E')$ are the shield media macroscopic cross sections. The $\sigma_{jk}(\boldsymbol{\Omega}, \boldsymbol{\Omega}', E, E')$ represent all those processes by which type k particles moving in direction $\boldsymbol{\Omega}'$ with energy E' produce a type j particle in direction $\boldsymbol{\Omega}$ with energy E (including decay processes). We solve equation (1) by a physics perturbation expansion (atomic, elastic, nuclear) with moment methods and asymptotic expansions for forward components followed by a collisional perturbation theory and multigroup/collocation/Legendre expansion methods for the diffuse components. Recent additions to the procedures are energy straggling, fragmentation energy widths and downshifts, and multiple scattering. The recently derived straggling parameter for protons is shown in fig. 1 in comparison to low energy proton straggling experiments where agreement with the new theory is demonstrated to near end of range for the first time.

The new Green's function for energy-loss/straggling has been used to analyze the transmission properties of the Shuttle spacesuit garment under low energy proton irradiation revealing the role of the non-uniformity of the water filled cooling tubes and porosity of the garment fabric. The proton spectrum on the target is shown as the right peak in Fig. 2. Only that fraction of garment not covered by the cooling tubes where transmission only through the fabric gives rise to the next highest energy peak. The greater width of the fabric related peak is due to the porosity of the fabric in addition to straggling effects. The broad spectral feature to the left

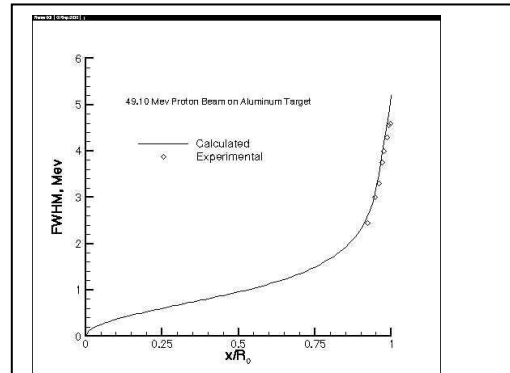


Fig. 1. FWHM of 49.1 MeV protons in an aluminum target.

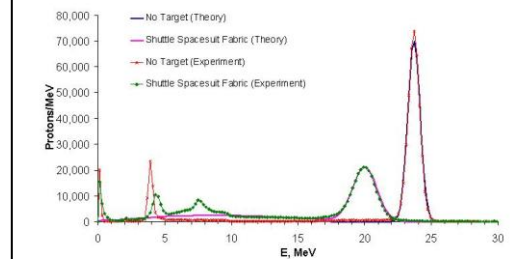


Fig. 2. Spacesuit garment transmission properties (experiment and theory).

of the two peaks is due to the geometry of the cooling tubes. The experimental/theoretical differences in this broad central region are believed due to multiple scattering effects. The rise in the spectrum at lowest energies results from atomic collisional equilibrium where the spectrum approaches an inverse stopping power distribution independent of the source spectrum. These results gave rise to a new spacesuit radiation analysis model and guides the development of future spacesuit designs. The effects of straggling on a monoenergetic beam of Ne is shown in Fig. 3. It is clear that straggling effects are important in analysis of HZE transmission properties in addition to the importance on low energy proton transmission properties.

The energy spread and energy downshifts in nuclear fragmentation events have been added to the first asymptotic expansion term, which is evaluated using collisional perturbation theory. The first three collisional perturbations of the first order asymptotic expansion is shown in Figs. 3 to 5. The first asymptotic correction term includes transverse spread of the beam due to multiple scattering and the transverse momentum spread in fragmentation. Although straggling is important in the energy spectrum of the transmitted primary beam as shown in Fig. 3, straggling is of minor importance in the higher order collisional terms shown in Figs. 4 and 5. These transported spectral widths are dominated by the effects of the fragmentation energy widths.

We rewrite equation (1) in operator notation in which the field functions $\phi_j(x, \Omega, E)$ are combined in a vector array Φ as

$$\Phi = [\phi_j(x, \Omega, E)] \quad (2)$$

with the drift term replaced by a diagonal matrix operator as

$$D = [\Omega \bullet \nabla] \quad (3)$$

and the interaction kernel into an operator containing diagonal $[\sigma_j(E)]$ and lower triangular elements related to $\sigma_{jk}(\Omega, \Omega', E, E')$ given as

$$I = [\sum] \sigma_{jk}(\Omega, \Omega', E, E') d\Omega' dE' - \sigma_j(E) \quad (4)$$

The interaction operator I has three parts associated with atomic, elastic, and reactive processes. Equation (1) is then rewritten with each contribution (atomic, elastic, reactive) shown separately as

$$[D - I_{at} - I_{el}] \bullet \Phi = I_r \bullet \Phi \quad (5)$$

where the first two physical perturbation terms (also diagonal operators) are shown on the left-hand side and have been adequately resolved in past research. The reaction cross section is separable into diffuse and forward components (Fig. 6 as example) for which equation (5) may be written as coupled equations

$$[D - I_{at} - I_{el} + \sigma_r] \bullet \Phi_{for} = \{ \int \sigma_{r,for}(\Omega, \Omega', E, E') d\Omega' dE' \} \bullet \Phi_{for} \equiv \mathcal{E}_{r,for} \bullet \Phi_{for} \quad (6)$$

and

$$\begin{aligned} [D - I_{at} - I_{el} + \sigma_r] \bullet \Phi_{iso} &= \{ \int \sigma_r(\Omega, \Omega', E, E') d\Omega' dE' \} \bullet \Phi_{iso} + \{ \int \sigma_{r,iso}(E, E') d\Omega' dE' \} \bullet \Phi_{for} \\ &\equiv \mathcal{E}_r \bullet \Phi_{iso} + \mathcal{E}_{r,iso} \bullet \Phi_{for} \end{aligned} \quad (7)$$

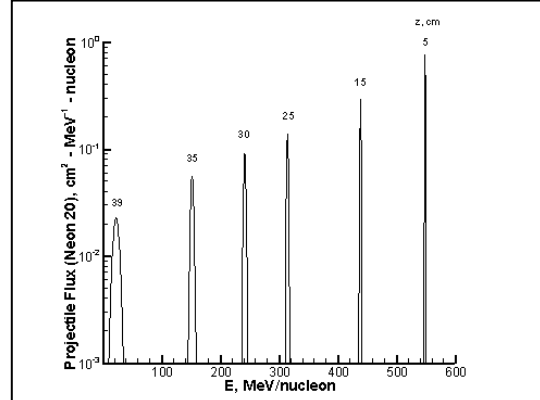


Fig. 3. Primary ion flux at various depths for Ne(20,10) incident on aluminum at 600 MeV/amu.

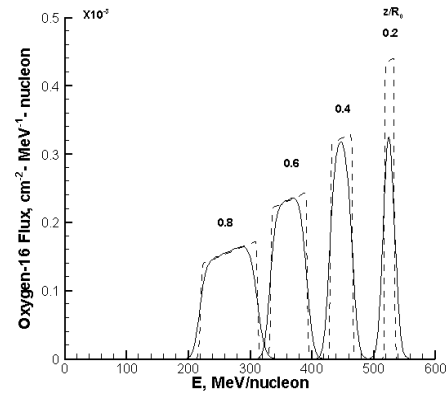


Fig. 4. First generation O(16,8) fragment flux at various depths compared with the same flux for the case in which the interaction energy width is zero (broken curve).

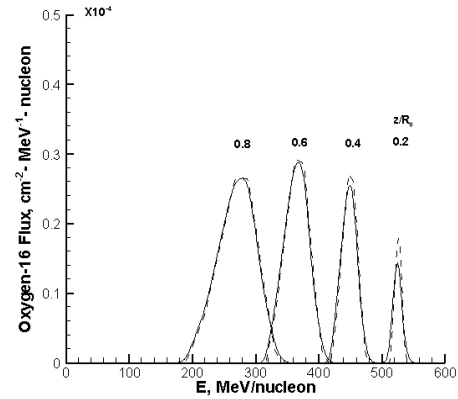


Fig. 5. Second generation O(16,8) fragment flux at various depths compared with the same flux for the case in which the interaction energy width is zero (broken curve).

where $\Phi = \Phi_{for} + \Phi_{iso}$ and the operator \mathcal{E}_r is the integral portion of I_r . Equation (6) is a Volterra equation and can be solved as a Neuman series which can be either evaluated directly or proscribed as a marching procedure in either a perturbative sense as the current form of HZETRN or nonperturbative sense (future version of HZETRN) as described elsewhere. The cross term in equation (7) gives rise to an isotropic source of light ions and neutrons of only modest energies. Spectral contributions to the Neuman series depend on the particle range and probability of surviving nuclear reactions which establish the form of the G matrix as ($G = [D - I_{at} - I_{el} + \sigma_r^{-1}]$), the inverse of the differential operator on the left of equations (6) and (7). The second term of the Neuman series is proportional to the probability of nuclear reaction that is limited by the particle range as discussed above. It is well known that nuclear reactions for the charged particles below a few hundred A MeV are infrequent for which rapid convergence of the collisional perturbation series has been demonstrated.

The remaining problem is solution for the transport of the low-energy neutron and light ion isotropic sources in equation (7) that dominate the solution below about 70 A MeV. In this region light ion transport is completely dominated by the atomic interaction terms and only a very small fraction have nuclear reactions making only minor contributions to the particle fields. This is especially true for the target fragments, which can be solved in closed form.

The neutrons have no charge and are dominated at low energies by elastic and reactive nuclear processes. We further expand equation (7) for the single neutron component as

$$[\Omega \cdot \nabla + \sigma_n] \phi_n(x, \Omega, E) \equiv \int \sigma_{nn}(\Omega, \Omega', E, E') \phi_n(x, \Omega', E') d\Omega' dE' + [\mathcal{E}_{r,iso} \cdot \Phi_{for} + \mathcal{E}_r \cdot \Phi_{(12)}]_n \quad (8)$$

where the last term is from coupling to the solution of equation (7). The neutron spectrum is greatly degraded in energy on the first collision and what remains of the low-energy neutron transport is the last issue to be resolved. This is the typical nuclear engineering problem for which a multitude of methods have been developed such as the Sn, multigroup, and collocation methods already applied to versions of HZETRN. It is mainly a question of computational efficiency and we continue to investigate this issue. Monte Carlo methods have been helpful in evaluation of these computational procedures in simple geometry where computational times differ by only 3 orders of magnitude. Results of the forward/backward method (fb) is compared to the Legendre expansion (Pn) method using the HZETRN nuclear database in Fig. 7. The Sn method is compared to MCNPX calculations using the ANISIN neutron database. It is clear that an improved database for HZETRN is required.

Introduction of multiple scattering Green's function is the next logical step in the sequential development of high speed computational procedures. We will utilize the multiple scattering solutions of Fermi given by

$$G(z, r, \theta_r) = [\sqrt{3} w^2 / 2\pi z^2] \exp[-w^2(\theta_r^2/z - 3r\theta_r/z^2 + 3r^2/z^3)]$$

Where z is the longitudinal distance and r is the lateral distance and θ_r is the angle to the longitudinal axis. We will be using Schimmerling and coworkers modifications to Fermi's width formula.

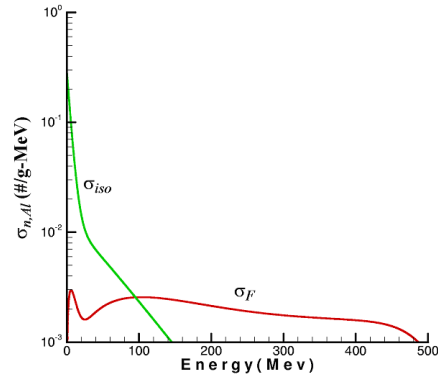


Fig. 6. Isotropic and forward neutron spectra produced by 500 MeV neutrons in aluminum.

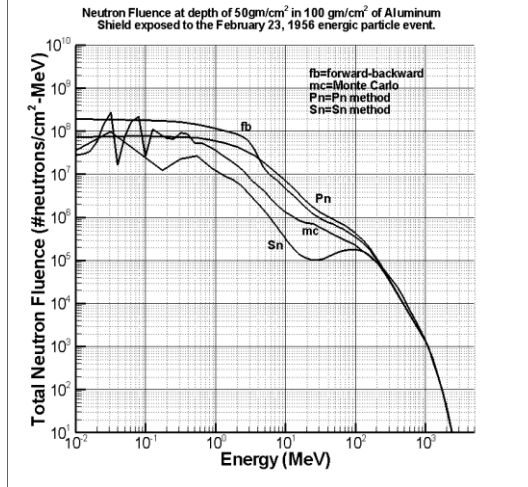


FIG. 7. Total neutron fluence at a depth of 50gm/cm² in 100 gm/cm² of aluminum shield exposed to the February 23, 1956 solar particle event